IEEE Access
Multidisciplinary | Rapid Review | Open Access Journal

Received March 25, 2020, accepted March 31, 2020, date of publication April 6, 2020, date of current version April 21, 2020.

Digital Object Identifier 10.1109/ACCESS.2020.2985711

A Three-Port Zero-Power RFID Sensor Architecture for IoT Applications

NABIL KHALID, (Student Member, IEEE), RASHID MIRZAVAND, (Senior Member, IEEE), HOSSEIN SAGHLATOON, (Member, IEEE), MOHAMMAD MAHDI HONARI, (Member, IEEE), AND PEDRAM MOUSAVI, (Senior Member, IEEE)

Intelligent Wireless Technology Laboratory, University of Alberta, Edmonton, AB T6G 2R3, Canada

Corresponding author: Nabil Khalid (nkhalid1@ualberta.ca)

This work was supported by the NSERC-AITF Industrial Research Chair Program.

ABSTRACT A novel zero-power wireless sensor architecture is proposed and demonstrated in this paper. The proposed wireless sensor, which is a passive sensor, combines UHF RFID and a capacitive sensor to enable reading of physical and chemical parameters wirelessly, without compromising much on the read-range, and complexity of conventional RFID tags. The sensor alters the phase of backscattered RFID signal, which is detected at the receiver using a non-coherent IQ demodulator. Due to the universal nature of this architecture, any type of sensor, such as temperature, humidity, water level sensor, can be realized. For the sake of simplicity, a varactor diode was initially used to get a thorough understanding of the system. Following that, a flood sensor was used to evaluate the performance of zero-power wireless sensor in a real-world application.

INDEX TERMS Backscattering, capacitive sensor, IoT, passive sensing architecture, radio frequency identification (RFID), RF sensor, ultra high frequency (UHF), wireless sensor, zero-power sensor.

I. INTRODUCTION

Wireless sensors are rapidly becoming an integral part of our daily lives. They are widely being used to determine everyday useful information ranging from monitoring temperature in a room to measuring fluid levels in different industries [1]–[4]. Their widespread usage has become possible due to their inexpensiveness and ease of installation. With the advancements of the Internet of Things (IoT), the utilization of wireless sensors is expected to grow exponentially to an extent that they will become ubiquitous [5]. Owing to this fast-paced growth, it has now become a need of the hour that some sophisticated designs of wireless sensors be introduced that offer improvement in terms of implementation, performance and cost.

At a very fundamental level, a wireless sensor is simply expected to identify a node and send a sensed parameter wirelessly to a base station. Thus, there are three major components of its operation: communication, identification and parameter sensing [6]. To perform these operations, energy is required by a sensor. Whatever technique is used to provide this energy directly influences the cost, life-span, wireless operable range, and circuit complexity [7]–[10].

One method to provide energy to a sensor node is adding a battery to it, which could be utilized to perform all the required operations. Although the wireless range of a battery-assisted sensor is very long, usually in tens of meters, the battery is actually a hurdle in a wireless sensor: it increases the cost of the system, it needs to be replaced every few months and it makes the sensor bulky [11]. Passive wireless sensors, on the other hand, harvest energy, which is sent by a reading device, and perform all the required operations. However, their range of operation is usually lower, up to a few meters [1]. Therefore, it is very important to engineer the hardware of battery-less wireless sensors in order to increase their working range.

Zero-power radio frequency identification (RFID) tag-based sensors, especially the ones operating in the ultra-high frequency (UHF) band, are gaining a lot of interest [10], [12]–[14]. Several designs have been proposed in the past. The simplest ones are chipless based RFID sensors in which no integrated circuit (IC) is required and the sensor data is determined by the change in the radar cross-section (RCS) of the RFID tag based on the sensed parameter [15]–[19].

The associate editor coordinating the review of this manuscript and approving it for publication was Xianfu Lei.

These are very low-cost passive wireless sensors; however, due to their analog communication nature, they are vulnerable to environmental effects and, additionally, they do not allow multiple tags to be placed in a single area. Chip-based tags, on the other hand, are considered a better candidate as they benefit from digital modulation, thus allowing the deployment of techniques such as coding and anti-collision, which enables reading of multiple tags simultaneously. In these sensors, usually matching network of RFID is used as a sensor. Any changes in the parameter of interest alters the operating frequency of the tag, thus causing alteration in the read-range at a given frequency. This technique requires measuring the amplitude of the backscattered signal at different frequencies to determine the sensed parameter and therefore it requires a wider spectrum [20]–[25]. A third type of battery-less sensors currently available in the market is the one that incorporates a digitization circuitry that uses off-the-shelf available sensors and digitally adds the sensed parameter's information to the backscattered RFID signal. However, this digital circuitry requires extra power, thus the read-range of the sensor drops to a distance (typically 0.7–2.2 meter) where the power received is adequate to run both the RFID and the digital circuitry [26]–[31]. To the best of author's knowledge, there is no RFID based sensor design that integrates a sensor passively without affecting the read-range of the RFID.

In this paper, we propose a novel wireless sensor architecture that successfully solves the challenges faced by wireless sensors. The proposed sensor architecture consists of a circulator, an antenna, an RFID chip and a capactive sensor. These components are connected in a sequence that the interrogation signal, which is being sent by a reader, is fed to the RFID to harvest energy. When the RFID responds back, the reflected signal is directed to the sensor before being returned back by the antenna. This sequencing is accomplished by using a circulator. The proposed sensor is capacitive in nature and thus it adds phase delay to the reflected signal, based on the sensor value. The signal is reflected by the sensor and reaches back to the reader after being radiated back by the antenna. It should be noted here that, since the sensor is physically separated in our architecture, unlike other previously discussed works on RFID based sensors, the radiation characteristics of the antenna and the performance of RFID such as read-range are not compromised by the changes in the parameter being sensed [20]–[22].

At the reader, the phase delay due to the changes in physical or chemical parameters experienced by the sensor, can be easily determined by using a non coherent IQ demodulator. These demodulators are widely available in commercial RFID readers. Therefore, by using this technique, cost of the sensors can be significantly reduced without compromising much on the working range and complexity. This new design can open door for several new applications ranging from personal use to industrial ones. An illustration in Fig. 1 shows a humidity sensor and a temperature sensor being used in a medical room to observe the environment, and a liquid level

FIGURE 1. Potential applications of zero-power wireless sensor network from determining environmental condition to healthcare monitoring.

detector being used to monitor the amount of dose given to the patient.

The goals of this research are threefold:

- propose an architecture for wireless sensors that provides longer range without requiring a battery at the node;
- using the phase of the backscattered signal for determining the sensing parameter in a passive manner;
- demonstrate its operation in a real world scenario.

The remainder of this paper is organized as follows. In Section II, we discuss the working principle of the sensor node. In Section III, the details of the proposed design are discussed. While, Section IV is dedicated to the discussion of the results. Finally, the paper is concluded in Section V.

II. WORKING PRINCIPLE

UHF RFID setup generally consists of two components: an interrogator, which reads information of an RFID tag; a tag, which keeps the tag ID and responds back to an interrogator. The interrogator, sometimes also referred to as a reader, transmits an RF signal for a small duration of time. This signal serves three purposes. The first is to energize the tag by transmitting an unmodulated RF signal. This energy is used to wakeup the tag. Following that, an interrogation signal is sent to request the tag to respond back. Finally, the tag responds by sending its ID.

Along with the tag ID, some other useful sensing information such as temperature, humidity, water level, moisture, flood etc. can also be included. This inclusion allows making a simple RFID a wireless sensor node. To send the information, the system requires some modifications based on the preference. The sensor information can either be sent back in digital or in analog domain. Digital transmission is generally more immune to noise however it also requires more power. Analog communication, on the other hand, is more power efficient. In a scenario where nodes are powerless, power efficiency of the system is paramount. Therefore, analog communication is selected in our case.

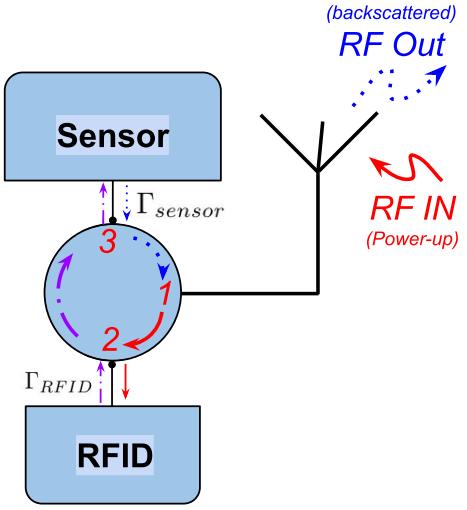

FIGURE 2. Block diagram of proposed zero-power wireless sensor.

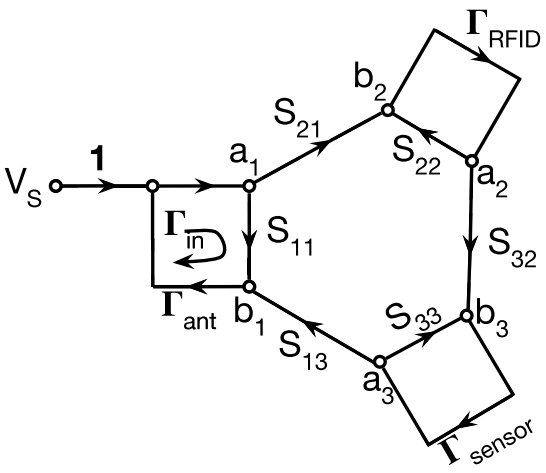

FIGURE 3. Signal flow graph of the sensor when RFID is in the reflecting state.

To realize the system, the power being reflected by the tag is sent through a capacitive sensor on its way back to the reader. The block diagram is shown in Fig. 2. As a result, the sensor adds some extra phase delay, depending on the condition of the sensor, which allows reading the sensor value at the reader, without compromising any power. Thus, the addition of sensor to the system doesn't theoretically reduce the read-range of the RFID tag.

Reading the phase at the reader is accomplished by a non-coherent IQ demodulator, which is in-built in almost every commercially available reader. The reader mixes an in-phase and a quadrature version of the transmitted signal with the received one and determines the amplitude of the output. These amplitudes are eventually used in determining the phase of the received signal.

To achieve the required specifications, a three-port system was developed, for which the details are provided in the following section.

III. SYSTEM DESIGN

The proposed system is an integration of an RFID and a sensor in a three-port structure. In order to understand the system, we will first discuss the three-port structure and then the whole system.

A. THREE-PORT STRUCTURE

A three-port RFID structure uses a non-reciprocal device to send the backscattered signal from the RFID to a different port, which is connected to a sensor. The signal after entering the sensor is reflected back from it with a change in phase, based on the sensed value. It should be noted here that, since the sensor is capacitive, the loss of signal power is minimal. This attribute is highly desirable for a battery-less sensor.

The required characteristics of a three-port structure are obtained in a circulator. A circulator is a nonreciprocal device that allows power flow between ports in a certain direction only. The direction of power flow depends on its construction and can be either clockwise or counterclockwise. For a typical circulator offering clockwise circulation, with every port matched, the scattering matrix is given by [32],

$$\mathbf{S_{circulator}} = \begin{bmatrix} 0 & 0 & 1 \\ 1 & 0 & 0 \\ 0 & 1 & 0 \end{bmatrix}. \tag{1}$$

During the power up state, when RFID is storing energy, all the power is sent to the RFID, which acts as a matched load. Thus the scattering matrix of the three-port structure is considered as (1). However, in case when the RFID is reflecting the signal for communication, the scattering matrix is no more the same. A signal flow graph, shown in Fig. 3 can be used to determine the characteristics of the system.

The signal that is reflected by the sensor is formulated as follows:

$$\Gamma_{in} = \frac{b_1}{a_1} = S_{11} + \frac{S_{13}S_{32}S_{21}\Gamma_{RFID}\Gamma_{sensor}}{(1 - S_{33}\Gamma_{sensor})(1 - S_{22}\Gamma_{RFID})}, \tag{2}$$

where S_{ij} are the scattering parameters of the circulator, Γ_{RFID} and Γ_{sensor} are the reflection coefficient of the RFID chip and sensor, respectively.

For the case when $S_{11} = S_{22} = S_{33} = \Gamma_{ant} = 0$ and $S_{13} = S_{32} = S_{21} = 1$, then the input reflection coefficient is given by

$$\Gamma_{in} = \frac{b_1}{a_1} = \Gamma_{RFID}\Gamma_{sensor}. \tag{3}$$

Considering the RFID and the sensor to be perfectly reflective (lossless), we get

$$\Gamma_{in} = e^{j(\theta_{RFID} + \theta_{sensor})}, \tag{4}$$

where, θ_{RFID} and θ_{sensor} are the phase delay caused by the RFID and the sensor, respectively. Here, θ_{RFID} depends on the distance between the RFID and the reader and is a known parameter. Whereas, θ_{sensor} is the phase delay caused due

to the capacitance of the sensor. This capacitance depends on the physical parameters that a sensor is reading. The resulting phase delay can be easily read at the reader, which is explained later.

A circulator can be physically realized in different ways, such as Ferrite core, directional coupler with a mismatched port, etc. For simplicity, we have used a low-cost ferrite-core clockwise circulator, SKYFR-001400 from Skyworks, that offers very low insertion-loss, less than 0.5 dB [33].

B. CAPACITIVE SENSOR

Sensors could be designed to be either resistive, in which resistance changes with the change in the physical parameter, or reactive, in which reactance changes with the change in the physical parameter. The former ones are usually lossy and not preferred when energy efficiency is a concern. In the latter ones, since only the reactance of the sensor changes ($Z = \pm jX$), they are more energy efficient. In capacitive sensors, usually change in parameter of interest causes permitivity variation that results in a change in the capacitance ($C = \epsilon \frac{d}{a}$). Therefore, they are a good candidate for a battery-less wireless sensor.

Capacitive sensors are widely available in the market. However, their operating frequency range is low, usually in the order of tens of kilohertz. Therefore, for a sensor to operate in the proposed system, new sensors with simple configuration were designed.

For thorough understanding of the system, first a varactor diode circuit was utilized to mimic a capacitive sensor. These diodes have a wide tuning range from 1 pF to 53 pF at 915 MHz. They provide important information regarding the behavior of the system such as the amount of phase change per picofarad. The circuit design consists of a simple biasing network and a DC-blocking capacitor. An illustration is shown in Fig. 4 (a).

Another sensor was designed to determine flooding in a given region. In the flood sensor, a design with two closely-spaced electrodes is used to form a capacitor. As the water level rises, the average permitivity of the capacitor changes, which in turn changes the capacitance of the sensor.

Finally, this change is superimposed on the RFID signal by altering the phase of the backscattered signal from the tag and can be easily read at the reader. An illustration of the sensor is shown in Fig. 4 (b).

C. RFID MATCHING NETWORK

The RFID tag used for proving our concept was Higgs-4 by Alien in a SOT 323 packaging [34]. It is a highly integrated single chip IC that operates at UHF frequencies. The IC is designed to meet the standards of EPC Gen 2. The minimum required power to wakeup this IC is -18.5 dBm. The operating frequency of the IC spans from 840 MHz to 960 MHz with an equivalent parallel RC circuit at its input. The resistance and the capacitance of the IC are 1.8 kΩ and 0.95 pF, respectively.

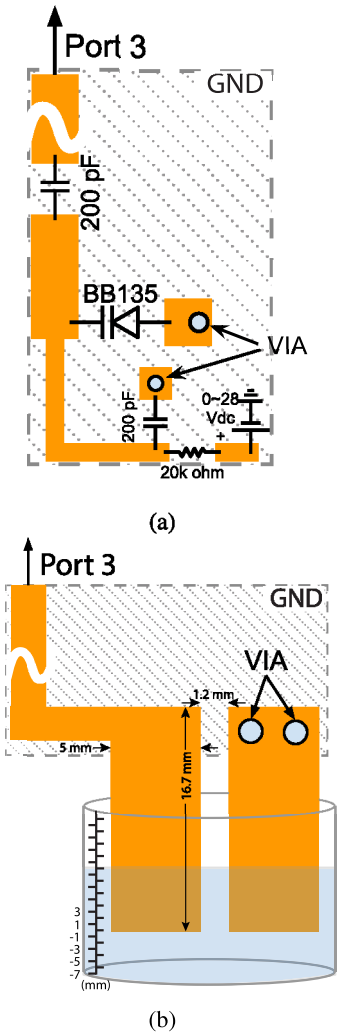

FIGURE 4. Sensor topologies: (a) varactor (b) flood.

In order to connect the IC to the system, a matching network is required to transform the tag impedance to 50 Ω to match it to the impedance of the circulator. A differential or non-differential matching network may be designed. A differential matching network provides out of phase signals at the input of the IC and thus develops higher voltage difference at the input pins but at the expense of complexity. For simplicity, we used non-differential matching network in which one port of the IC was grounded and other was attached to a matching network, which was designed to match the tag's input impedance, from $Z_{in} = 18 - j181$ Ω at 915 MHz to 50 Ω. A single-stub matching network with open circuited series stub was used for the matching [32]. The network was initially designed using a smithchart for 50 Ω transmission lines with distance from load to stub as 83.716 degrees, while the open-circuited stub was calculated to be 80.737 degrees. A schematic is shown in Fig. 5.

To realize the circuit, the stubs were first meandered and then optimized to cover the whole bandwidth from 902 MHz to 928 MHz using Keysight's Advanced Design System, version 2019. The optimizer was set to vary the stubs' widths

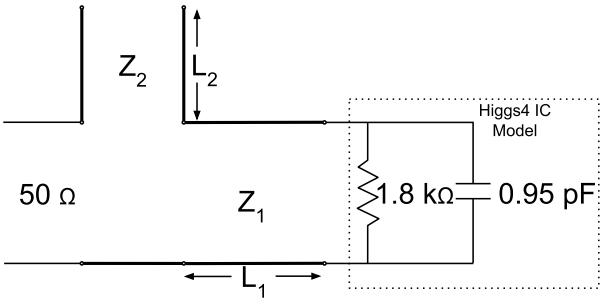

FIGURE 5. Schematic of the single-stub design used to match the RFID to 50 ohms.

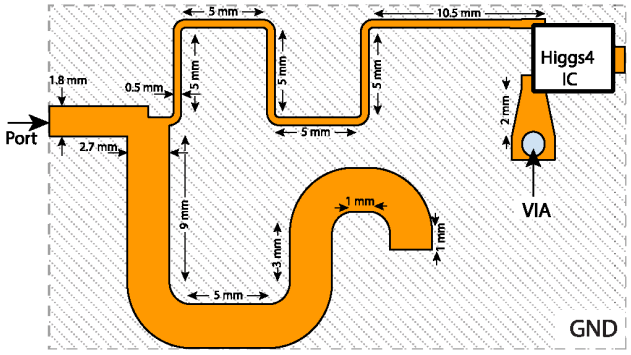

FIGURE 6. Final miniaturized and optimized version of the matching circuit of the Higgs 4 IC that utilizes microstrip technology to match the IC to 50 ohm impedance.

and lengths using the Least Pth algorithm until the reflection coefficient of less than −10 dB for the whole bandwidth was achieved. The final optimized circuit was fabricated on an RO4003C substrate with relative permittivity (ϵ_r) of 3.38, thickness of 0.81 mm and loss tangent ($tan\delta$) of 0.0027. The final miniaturized circuit, with all the physical dimensions, is shown in Fig. 6.

D. SYSTEM INTEGRATION

For a clockwise ferrite core circulator, each individual component must be connected in a proper sequence to have optimum performance. An antenna may be connected to the port 1 of the circulator. If so, the RFID tag with its matching network must be connected to the following port, in the clockwise direction, i.e. port 2. Finally, sensor is connected to the last remaining port, as shown in Fig. 2. The final integrated system is shown in Fig. 7.

The reason for connecting sensor after the RFID is as follows. Normally, a capacitive sensor is considered lossless, however, practically, it may have some losses. If the signal from the reader is sent to the sensor before it is sent to the RFID tag, it will be attenuated. As a result, signal reaching the RFID terminals will be smaller in amplitude. Thus, the RFID will store less energy.

On the other hand, if the sensor is connected after the RFID, in the circulator, the RFID wakes up with a stronger signal resulting in a higher read-range. In this case, the only loss a power-up signal faces is the circulator's insertion loss,

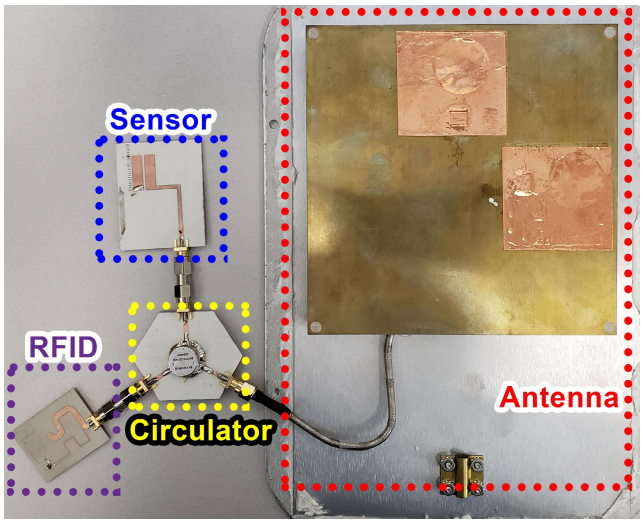

FIGURE 7. Final fabricated design of zero-power wireless sensor.

which is only 0.5 dB. Whereas losses in the backscattered signal will include: imperfect reflection from the tag; circulator's insertion loss from tag to the sensor; sensor loss and circulator's insertion loss from sensor to the antenna. As the sensitivity level of a typical reader can be as low as −90 dBm, backscattered signal being attenuated can be tolerated. Therefore, this observation confirms that charging the RFID tag is a limiting factor and advices that the capacitive sensor should be connected after the RFID to avoid any loss in the signal being received by the tag for the power-up purposes.

The overall power-up signal loss in this configuration can be determined as follows. Keeping in mind that the insertion loss of the circulator is 0.5 dB, to receive −18.5 dBm at the RFID tag, we need to make sure that the node receives a signal power of −18 dBm (0.5 dB higher than the tag). Using the Path loss formula, we can find that a 0.5 dB of path loss is incurred for a distance of 27.6 mm. Therefore, the reduction in the distance of the RFID in the proposed configuration is simply 0.027 meters, which is negligible in our case.

E. READER

The reader used in our experiments was AS3993 Fermi evaluation kit that included all the components and was able to provide up to 22 dBm of output power (extendable to 30 dBm for longer range) [35]. It includes a combination of a directional coupler and a low pass filter to separate the transmitted signal with the received one. The received signal is fed to a non-coherent in-phase (I) and quadrature (Q), IQ, mixer and sampled by an ADC to determine the strength of the IQ components of the signal independently. By applying a simple trigonometry, $\tan^{-1}(\frac{Q}{I})$, the phase of the received signal is determined.

Finally, the phase delay caused due to the setup and distance between the RFID reader and the tag, which is θ_{RFID}, is nullified by calibrating the system using a known capacitance value attached to the RFID. Following that, the extracted phase value is transformed into the respective

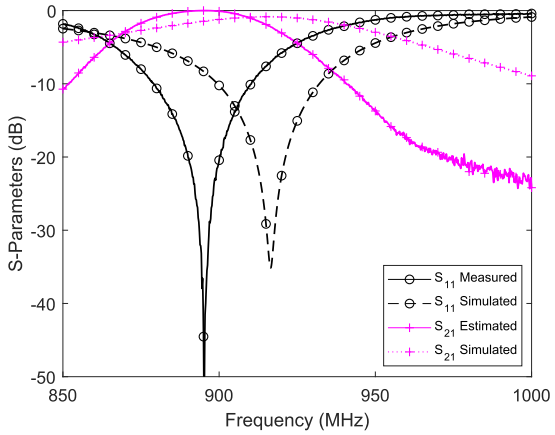

FIGURE 8. Frequency response of the RFID matching circuit.

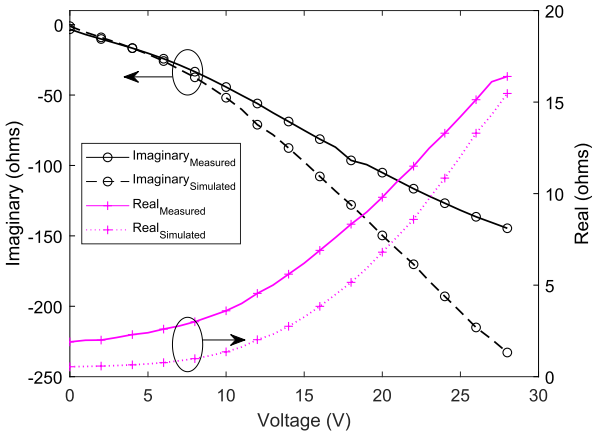

FIGURE 9. Impedance response of the varactor at 915 MHz.

parameter, such as voltage in case of the varactor or the water level, in case of the flood sensor, to determine the state of the physical parameter of interest.

IV. RESULTS

A. INDIVIDUAL COMPONENTS

In this subsection, the performance of individual components is discussed and a comparison between the simulated and the measured results is shown.

As a first step, performance of the designed RFID matching circuit was determined by measuring its scattering parameters. Although the simulated circuit was designed to be matched at 915 MHz, the measured response of the fabricated circuit was found to be shifted to 895 MHz. This shift did not have severe effects on the performance of the system when operating at 915 MHz. The scattering parameters are shown in Fig. 8. Here, the input is marked as port 1 and the resistance of the RFID is marked as port 2. As port 2 does not exist in reality, an estimated response, S_{21} Estimated, was calculated using the S_{11} Measured. This helps in determining the power transfer to the RFID at different frequencies.

Since the performance of the proposed sensing structure is aimed to be demonstrated by the change in the capacitive load (varactor diode), the characterization of the varactor diode is required. Figure 9 shows the simulated and measured results of the impedance response of the NXP BB135 varactor diode [36]. The discrepancies between the simulated and measured results can be attributed to the fact that a high frequency model of the varactor diode was not used. However, the deviation is small at lower voltages, i.e. from 0 to 10 volts.

Using the above results, a mathematical model between the phase of the reflected signal and voltage was developed using the process of curve fitting and reported by the following equation,

$$C = 3.314 \times 10^{-11} e^{-1.218V} + 1.978 \times 10^{-11} e^{-0.1748V}, \quad (5)$$

and for a perfectly reflective capacitor,

$$\angle\Gamma = \tan^{-1} \frac{-2\omega C Z_o}{1 - (\omega C Z_o)^2}, \quad (6)$$

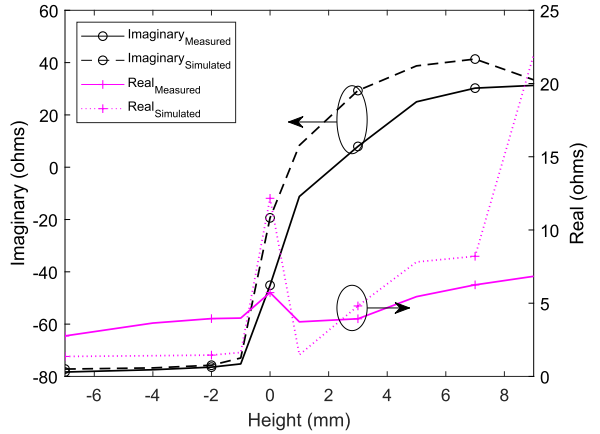

FIGURE 10. Impedance response of the flood sensor at 915 MHz as the level of the water changes while keeping the electrodes 7 mm above the base of the container.

where, $Z_o = 50\Omega$, $\omega = 2\pi f$, V is the voltage applied across the varactor and C is the capacitance of the varactor. These equations are useful in predicting the change in the phase of the reflected signal for voltages ranging from 0 to 10 volts.

The flood sensor was also fabricated on the same substrate. The impedance response of the sensor with respect to increasing water levels was recorded and the results are presented in the Fig. 10. The measured results are compared with the simulated results that were obtained by performing a full 3D EM simulation. The sensor was designed to have 7 mm empty space below the electrodes. Thus the actual electrodes were 7 mm above the base of the container. As the water level increases, a change in the reactance of the sensor can be seen. The change is significant as the water reaches closer to the electrodes at $h = 0$ mm. It can also be seen that the resistance of the sensor also starts increasing as the level of the water increases. This, in turn, may result in the reduction of the range and, therefore, its use should be avoided in this region if long range is a concern.

A mathematical relation between phase of the reflected signal and voltage was found by developing the following

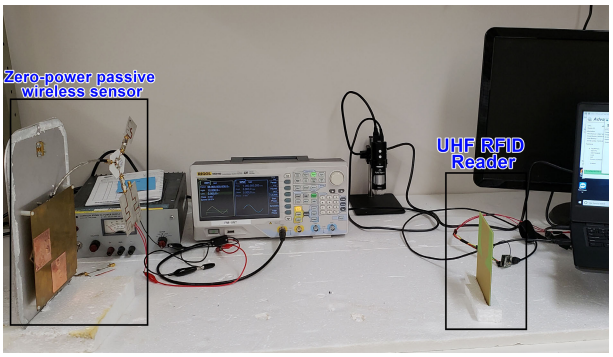

FIGURE 11. Zero-Power wireless RFID sensor with varactor attached at the sensor port.

exponential curve,

$$X_c = \begin{cases} 0.483h - 75.17 & -\infty < h < -1 \\ -75.06e^{-0.3893h} + 34.4 & -1 \leq h < 9. \end{cases} \quad (7)$$

Using the relation $C = 1/\omega X_c$, we can again use (6) to predict the phase change with respect to the change in the height of the water.

B. FULL RFID SYSTEM

We will now show the full zero-power wireless sensor setup and its performance. The setup consists of a reader, that measures the phase change and the proposed zero-power wireless sensor. For initial testing, the varactor diode was attached and the response of the system was observed. The setup is shown in Fig. 11 and the results are shown in Fig. 12. A clear one to one relation can be seen in the results. Small variations in the results are expected since in order to mimic a realistic scenario, the experiments were performed on a metallic table without the use of RF absorbers.

In the initial test, a triangular voltage was applied across the varactor diode to change its capacitance from 53 pF to 3 pF at 915 MHz. The corresponding voltages were between 0 and 10 volts. It can be observed from Fig. 12 that the phase at the reader changes as the voltage across the varactor diode is varied. Initially, when the time is 0 sec, the voltage is at 5 volts and the phase is 49 degrees. Next, when the voltage reaches its maximum value of 10 volts, the phase also reaches its maximum value of 75 degrees. Similarly, when the voltage across varactor reaches 0 volts, the phase at the reader is read as 23 degrees. The multiple sweeps show how repeatable the values are. An estimated phase, that was calculated using (6) and (5), is also shown in Fig. 12 to compare the simulated and measured results.

The proposed sensor was found to be working up to 7 meters. This was also verified through simple calculations. We need −18.5 dBm to power-up the tag. Therefore, the maximum acceptable path loss can be calculated using the following relation: −18.5 dBm = 22 dBm (reader power) + 2.1 dBi (reader antenna gain) − PL + 6.5 dBi (tag antenna gain) − 0.5 dB (circulator insertion loss) which leads to PL = −48.6 dB. At 915 MHz, this path loss is incurred for a distance of 7 meters.

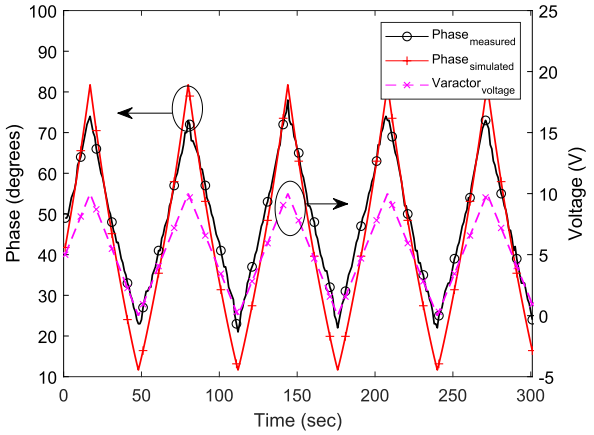

FIGURE 12. Measured phase change at the receiver as the voltage across varactor is changed with respect to time.

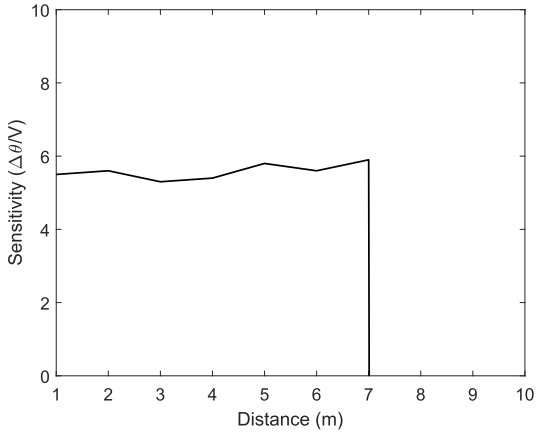

FIGURE 13. Sensitivity of the sensor at various distances.

The experiments were repeated at different distances, ranging from 1–7 meters, to find out the sensitivity of the sensor, while the Tx power level was set to 22 dBm. As shown in Fig. 13, no noticeable change in the results was observed. The reason that the sensitivity remains unchanged is attributed to the fact that the charging of the tag is currently the limiting factor and it does not allow the reading of the sensor node at distances where the reflected signal would reach close to the sensitivity level of the reader.

This behavior could be further explained by considering the following situation. The RFID tag in the sensor node must operate until it receives the minimum required, power-up signal, of −18.5 dBm. Considering the worst case scenario of the tag being at a distance of 7 meters, the backscattered signal received at the receiver can be calculated using the following relation: P_{rec} = −18.5 dBm (minimum required power of the power-up signal) − 1 dB (loss due to imperfect reflection from the tag [37]) − 0.5 dB (circulator's insertion loss) − 1.5 dB (loss in the sensing element) − 0.5 dB (circulator's insertion loss) + 6.5 dBi (tag antenna gain) − 48.6 dB

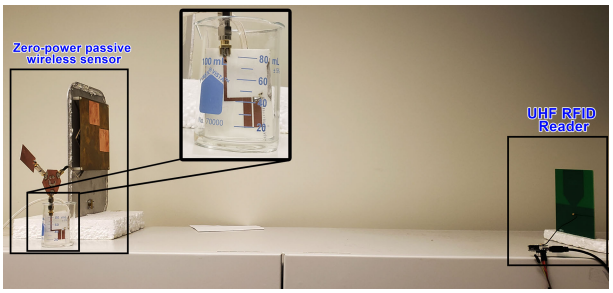

FIGURE 14. Zero-Power wireless RFID sensor with flood sensor attached at the sensor port.

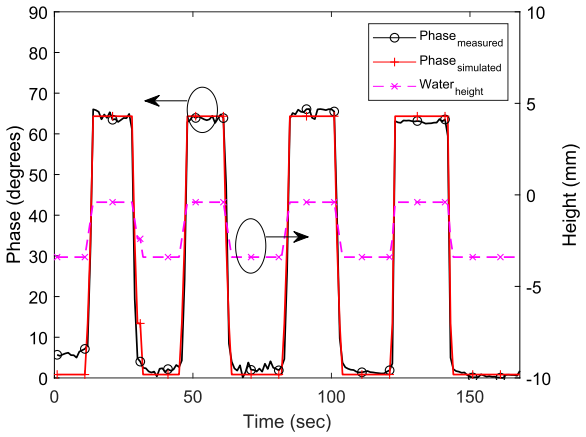

FIGURE 15. Performance of flood sensor shown by adding and removing water repeatedly.

(Path loss for 7 meters) + 2.1 dBi (reader's antenna gain). Therefore, the signal strength of the backscattered signal is calculated as −62 dBm. Nevertheless, the backscattered signal of −62 dBm, is still much higher than the sensitivity of the reader, which is −90 dBm. Therefore, the sensitivity of the sensor node remains unchanged for its distance of operation of 7 meters, and hence it can be said that the sensitivity of the proposed sensor is dependent on the receiver's sensitivity.

Finally, performance of the zero-power wireless sensors in a real-life application was observed. In this test, a flood sensor was used to determine the level of water in a beaker. The setup is shown in Fig. 14 and the results are shown in Fig. 15. Initially, there is no water in the beaker and the phase is calibrated to around 0 degrees. As soon as water is injected into the beaker, the phase delay increases as shown in Fig. 15. When the water level reaches the electrodes (h = 0 mm), the value reaches to around 65 degrees. For a comparison, phase calculated using (6) and (7) is shown in Fig. 15. The measured results are in a good agreement with the simulated ones.

To evaluate the performance of the sensor, the beaker was filled four times and the maximum value of all the four peaks were observed to be slightly different. This indicates that the sensor may not be used to accurately measure water levels, however, in case of flood sensing, a threshold value to 10 degrees is always observed to be crossed, thus a reliable flood sensing is possible.

TABLE 1. Comparison of the proposed system with other passive wireless sensors.

Parameter	This work	Chipless [15]–[19]	Chip-based [20]–[25]
Battery	No	No	No
Complexity	low	low	Medium
Sensing	Any	Any	Any
Multiple nodes	Yes	No	Yes
Anti-collision	Yes	No	Yes
Bandwidth required	∼KHz	∼MHz	∼MHz
Range (m)	7	30	3–5

All the above experiments were performed at a fixed distance from the reader. As the phase difference is dependent on the distance between the reader and the tag, the phase is expected to be different for different distances and is thus ambiguous for all the distances. To remove the ambiguity, phase difference between three frequencies, two closely spaced and one further, can be used to determine exact distance. Then the phase change due to distance can be adjusted to find the exact value of the sensor. Another method is to use a separate reference tag that is not affected by the environment. The phase difference between the reference tag and the sensor can be used to remove the phase ambiguity.

A comparison of the proposed zero-power wireless sensor with the other state-of-the-art wireless sensors is done in Table 1. It can be seen that the proposed sensor offers low complexity, and allows multiple nodes to operate simultaneously along with a good operating range of 7 meters.

V. CONCLUSION

In this paper, a novel zero-power wireless sensor is proposed that works without a battery. The proposed architecture integrates an RFID tag with a sensor and antenna using a circulator. The sensors, which are designed to be capacitive in nature, add phase delay to the signal transmitted by the UHF RFID tag based on the parameter that is being sensed by the sensor. A general system consisting of a varactor diode and a real system with a flood sensor are demonstrated. Results show that the architecture can be used to sense different parameters such as water level, flood and moisture. It was also discussed how this architecture provides longer range compared to other sensors available, without the use of batteries and thus can be used in several different applications ranging from healthcare, and industrial to smart home monitoring.

REFERENCES

[1] B. S. Cook, R. Vyas, S. Kim, T. Thai, T. Le, A. Traille, H. Aubert, and M. M. Tentzeris, "RFID-based sensors for zero-power autonomous wireless sensor networks," *IEEE Sensors J.*, vol. 14, no. 8, pp. 2419–2431, Aug. 2014.

[2] R. Mirzavand, M. M. Honari, and P. Mousavi, "Direct-conversion sensor for wireless sensing networks," *IEEE Trans. Ind. Electron.*, vol. 64, no. 12, pp. 9675–9682, Dec. 2017.

[3] R. Mirzavand, M. M. Honari, and P. Mousavi, "High-resolution dielectric sensor based on injection-locked oscillators," *IEEE Sensors J.*, vol. 18, no. 1, pp. 141–148, Jan. 2018.

[4] R. Mirzavand, M. M. Honari, and P. Mousavi, "High-resolution balanced microwave material sensor with extended dielectric range," *IEEE Trans. Ind. Electron.*, vol. 64, no. 2, pp. 1552–1560, Feb. 2017.

[5] O. Elijah, T. A. Rahman, I. Orikumhi, C. Y. Leow, and M. H. D. N. Hindia, "An overview of Internet of Things (IoT) and data analytics in agriculture: Benefits and challenges," *IEEE Internet Things J.*, vol. 5, no. 5, pp. 3758–3773, Oct. 2018.
[6] S.-M. Yu, P. Feng, and N.-J. Wu, "Passive and semi-passive wireless temperature and humidity sensors based on EPC generation-2 UHF protocol," *IEEE Sensors J.*, vol. 15, no. 4, pp. 2403–2411, Apr. 2014.
[7] R. Mirzavand, M. M. Honari, and P. Mousavi, "N-ZERO direct conversion wireless sensor based on six-port structures," in *IEEE MTT-S Int. Microw. Symp. Dig.*, Jun. 2017, pp. 1225–1227.
[8] M. M. Honari, H. Saghlatoon, R. Mirzavand, and P. Mousavi, "An RFID sensor for early expiry detection of packaged foods," in *Proc. 18th Int. Symp. Antenna Technol. Appl. Electromagn. (ANTEM)*, Aug. 2018, pp. 1–2.
[9] H. Saghlatoon, R. Mirzavand, M. M. Honari, and P. Mousavi, "Sensor antenna transmitter system for material detection in wireless-sensor-node applications," *IEEE Sensors J.*, vol. 18, no. 21, pp. 8812–8819, Nov. 2018.
[10] R. Mirzavand and P. Mousavi, "A ZERO-power sensor using multi-port direct-conversion sensing," *IEEE Sensors J.*, vol. 18, no. 22, pp. 9243–9250, Nov. 2018.
[11] O. B. Akan, O. Cetinkaya, C. Koca, and M. Ozger, "Internet of hybrid energy harvesting things," *IEEE Internet Things J.*, vol. 5, no. 2, pp. 736–746, Apr. 2018.
[12] R. Mirzavand, M. Honari, B. Laribi, B. Khorshidi, M. Sadrzadeh, and P. Mousavi, "An unpowered sensor node for real-time water quality assessment (humic acid detection)," *Electronics*, vol. 7, no. 10, p. 231, 2018.
[13] M. M. Honari, R. Mirzavand, H. Saghlatoon, and P. Mousavi, "A two-port microstrip sensor antenna for permittivity and loss tangent measurements," in *Proc. 13th Eur. Conf. Antennas Propag. (EuCAP)*, 2019, pp. 1–4.
[14] H. Saghlatoon, R. Mirzavand, M. M. Honari, and P. Mousavi, "Sensor antenna for dielectric constant measurement of materials in contact with the structure," in *Proc. 13th Eur. Conf. Antennas Propag. (EuCAP)*, 2019, pp. 1–3.
[15] T. T. Thai, H. Aubert, P. Pons, M. M. Tentzeris, and P. Robert, "Design of a highly sensitive wireless passive RF strain transducer," in *IEEE MTT-S Int. Microw. Symp. Dig.*, Jun. 2011, pp. 1–3.
[16] H. Aubert, F. Chebila, M. Jatlaoui, T. Thai, H. Hallil, A. Traille, S. Bouaziz, A. Rifai, P. Pons, P. Menini, and M. Tentzeris, "Wireless sensing and identification of passive electromagnetic sensors based on millimetre-wave FMCW RADAR," in *Proc. IEEE Int. Conf. RFID-Technol. Appl. (RFID-TA)*, Nov. 2012, pp. 398–403.
[17] B. S. Cook, A. Shamim, and M. M. Tentzeris, "Passive low-cost inkjet-printed smart skin sensor for structural health monitoring," *IET Microw., Antennas Propag.*, vol. 6, no. 14, pp. 1536–1541, Nov. 2012.
[18] X. Yi, C. Cho, C.-H. Fang, J. Cooper, V. Lakafosis, R. Vyas, Y. Wang, R. T. Leon, and M. M. Tentzeris, "Wireless strain and crack sensing using a folded patch antenna," in *Proc. 6th Eur. Conf. Antennas Propag. (EUCAP)*, Mar. 2012, pp. 1678–1681.
[19] S. Bouaziz, F. Chebila, A. Traille, P. Pons, H. Aubert, and M. M. Tentzeris, "Novel microfluidic structures for wireless passive temperature telemetry medical systems using radar interrogation techniques in ka-band," *IEEE Antennas Wireless Propag. Lett.*, vol. 11, pp. 1706–1709, 2012.
[20] B. S. Cook, J. R. Cooper, and M. M. Tentzeris, "An inkjet-printed microfluidic RFID-enabled platform for wireless lab-on-chip applications," *IEEE Trans. Microw. Theory Techn.*, vol. 61, no. 12, pp. 4714–4723, Dec. 2013.
[21] S. Kim, Y. Kawahara, A. Georgiadis, A. Collado, and M. M. Tentzeris, "Low-cost inkjet-printed fully passive RFID tags using metamaterial-inspired antennas for capacitive sensing applications," in *IEEE MTT-S Int. Microw. Symp. Dig.*, Jun. 2013, pp. 1–4.
[22] X. Chen, L. Ukkonen, and T. Björninen, "Passive E-textile UHF RFID-based wireless strain sensors with integrated references," *IEEE Sensors J.*, vol. 16, no. 22, pp. 7835–7836, Nov. 2016.
[23] H. He, X. Chen, L. Ukkonen, and J. Virkki, "Clothing-integrated passive RFID strain sensor platform for body movement-based controlling," in *Proc. IEEE Int. Conf. RFID Technol. Appl. (RFID-TA)*, Sep. 2019, pp. 236–239.
[24] X. Chen, H. He, Z. Khan, L. Sydanheimo, L. Ukkonen, and J. Virkki, "Textile-based batteryless moisture sensor," *IEEE Antennas Wireless Propag. Lett.*, vol. 19, no. 1, pp. 198–202, Jan. 2020.
[25] A. A. Kutty, T. Björninen, L. Sydänheimo, and L. Ukkonen, "A novel carbon nanotube loaded passive UHF RFID sensor tag with built-in reference for wireless gas sensing," in *IEEE MTT-S Int. Microw. Symp. Dig.*, May 2016, pp. 1–4.
[26] L. Yang, R. Zhang, D. Staiculescu, C. P. Wong, and M. M. Tentzeris, "A novel conformal RFID-enabled module utilizing inkjet-printed antennas and carbon nanotubes for gas-detection applications," *IEEE Antennas Wireless Propag. Lett.*, vol. 8, pp. 653–656, 2009.
[27] R. Vyas, V. Lakafosis, H. Lee, G. Shaker, L. Yang, G. Orecchini, A. Traille, M. M. Tentzeris, and L. Roselli, "Inkjet printed, self powered, wireless sensors for environmental, gas, and authentication-based sensing," *IEEE Sensors J.*, vol. 11, no. 12, pp. 3139–3152, Dec. 2011.
[28] AMS. *SL900A EPC Gen2 Sensor Tag*. Accessed: Apr. 9, 2020. [Online]. Available: https://ams.com/documents/20143/36005/SL900A_DS000294_5-00.pdf/d399f354-b0b6-146f-6e98-b124826bd737
[29] J. F. Salmerón, F. Molina-Lopez, A. Rivadeneyra, A. V. Quintero, L. F. Capitan-Vallvey, N. F. de Rooij, J. B. Ozáez, D. Briand, and A. J. Palma, "Design and development of sensing RFID tags on flexible foil compatible with EPC gen 2," *IEEE Sensors J.*, vol. 14, no. 12, pp. 4361–4371, Dec. 2014.
[30] J. Fernández-Salmerón, A. Rivadeneyra, F. Martínez-Martí, L. Capitán-Vallvey, A. Palma, and M. Carvajal, "Passive UHF RFID tag with multiple sensing capabilities," *Sensors*, vol. 15, no. 10, pp. 26769–26782, 2015.
[31] A. Falco, J. Salmerón, F. Loghin, P. Lugli, and A. Rivadeneyra, "Fully printed flexible single-chip RFID tag with light detection capabilities," *Sensors*, vol. 17, no. 3, p. 534, 2017.
[32] D. M. Pozar, *Microwave Engineering*. Hoboken, NJ, USA: Wiley, 2012.
[33] Skyworks. *Specification Sheet: SKYFR-001400: 925–960 MHz Sngle Junction Robust Lead Circulator*. Accessed: Apr. 9, 2020. [Online]. Available: https://www.skyworksinc.com/-/media/SkyWorks/Documents/Products/2401-2500/SKYFR_001400_2.pdf
[34] *Higg4 SOT Datasheet Addendum, Alien*. Accessed: Apr. 9, 2020. [Online]. Available: https://www.alientechnology.com/download/higgs-4-files/?wpdmdl=7563&ind=QUxDLTM3MC1TT1QgSGlnZ3M0IFNPVCAyMDE3LTAyLTEwLnBkZg
[35] AMS. *Application Note: UHF RFID Fermi Reader HW-Description*. Accessed: Apr. 9, 2020. [Online]. Available: https://media.digikey.com/pdf/Data%20Sheets/Austriamicrosystems%20PDFs/AS3993-DK-RB-FERMI_Rev1.0_2012-06-26.pdf
[36] *BB135—UHF Variable Capacitance Diode Product Specification, NXP*. Accessed: Apr. 9, 2020. [Online]. Available: https://www.nxp.com/docs/en/data-sheet/BB135.pdf?
[37] J. D. Griffin and G. D. Durgin, "Complete link budgets for backscatter-radio and RFID systems," *IEEE Antennas Propag. Mag.*, vol. 51, no. 2, pp. 11–25, Apr. 2009.

NABIL KHALID (Student Member, IEEE) received the bachelor's degree in electrical engineering from Air University, Islamabad, Pakistan, in 2013, and the M.Sc. degree in electrical and computer engineering from Koc University, Istanbul, Turkey. He is currently pursuing the Ph.D. degree with the Electrical and Computer Engineering Department, University of Alberta, Edmonton, AB, Canada, under the supervision of Prof. P. Mousavi. His majors involved telecommunications, RF/microwave, and RADARs. From 2013 to 2014, he worked as a Design Engineer with the RF/Microwave Department, RWR Pvt., Ltd., Islamabad, Pakistan. His focus was on designing industrial grade power amplifiers. From 2015 to 2017, he worked with the Next-Generation and Wireless Communications Laboratory (NWCL), as a Research Assistant. His focus was developing the physical layer of THz Band wireless communications. He joined as a Research Assistant with the Intelligent Wireless Technologies Laboratory (IWT), in 2017. He is focused on designing passive wireless sensors.

RASHID MIRZAVAND (Senior Member, IEEE) received the B.Sc. degree from the Isfahan University of Technology, in 2004, and the M.Sc. and Ph.D. degrees from the Amirkabir University of Technology, in 2007 and 2011, respectively, all in electrical engineering.

From 2012 to 2015, he was an Assistant Professor with the Amirkabir University of Technology. Since 2015, he has been a Research and Development Scientist. He is currently an Adjunct Professor with the Intelligent Wireless Technology Laboratory, University of Alberta, where he is also a Co-Founder of several companies. He is the author of more than 120 articles published in refereed journals and conferences proceedings. His research interests include microwave/mm-wave circuits, sensors, measurement systems, and antennas.

Dr. Mirzavand received the Best M.Sc. Researcher Award 2007, the Best Ph.D. Researcher Award 2011, the Best MICT National Researcher Award 2013, National the Elite Foundation Young Professor Grant Award 2014, AITF Elite PDF Award 2015, the Honorable CMC Industrial Collaboration Award 2017, and the TEC Edmonton Innovation Award 2019.

HOSSEIN SAGHLATOON (Member, IEEE) received the B.Sc. degree in electrical engineering from the Ferdowsi University of Mashhad, Mashhad, Iran, in 2012, the M.Sc. degree (Hons.) in RF electronics from the Tampere University of Technology, Tampere, Finland, in 2014, and the Ph.D. degree from the University of Alberta, Edmonton, AB, Canada, in May 2019.

He is currently a Postdoctoral Fellow with the Intelligent Wireless Technology Laboratory (IWT), University of Alberta, where he is also a Co-Founder of SenZioT Company. His research interests include advanced intelligent antennas, 3-D printable radio frequency electronics, RFID technology, RF/Microwave sensing, sensor communications, and the IoT. He was a recipient of the Distinction Graduation Award, in 2014, the Graduate Students' Association Professional Development Award, in 2015, the Graduate Student Association Travel Award, in 2016, the two years Alberta Innovates Technology Futures (AITF) Ph.D. Scholarship, in 2017, the Faculty of Graduate Studies and Research Travel Award, in 2018, the RR Gilpin Memorial Scholarship 2018, the GSA Graduate Student Research Assistant Award, in 2019, and the TEC Edmonton Innovation Award, in 2019.

MOHAMMAD MAHDI HONARI (Member, IEEE) received the B.Sc. degree from the Ferdowsi University of Mashhad, Mashhad, Iran, and the M.Sc. degree from the Amirkabir University of Technology, Tehran, Iran, in electrical engineering. He is currently pursuing the Ph.D. degree with the Intelligent Wireless Technology (IWT) Laboratory, University of Alberta, Edmonton, AB, Canada. His research areas include periodic structures, leaky-wave antennas, phased array antennas, sensors, and metamaterial. He received the Best M.Sc. Researcher Award in Telecommunications and the Best M.Sc. Thesis Award from the Amirkabir University of Technology, in 2012. He was a recipient of the Alberta Innovates Technology Futures (AITF) Scholarship, the Sadler Graduate Scholarship, the GSA Research Assistantship Award, and the Martha Piper Award in his Ph.D. program.

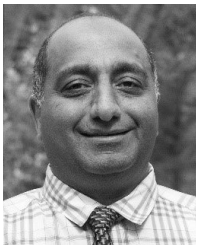

PEDRAM MOUSAVI (Senior Member, IEEE) received the B.Sc. degree(Hons.) in telecommunication engineering from the Iran University of Science and Technology, Tehran, in 1995, and the M.Sc. and Ph.D. degrees from the University of Manitoba, Winnipeg, Canada, in 1997 and 2001, respectively, all in electrical engineering.

He has more than 18 years of entrepreneurial academic experience with start-up companies from the University of Waterloo and the University of Alberta. He founded Intelwaves Technologies as a spin-off from the University of Waterloo. He is currently a Professor with the Department of Mechanical Engineering and the NSERC-AI Industrial Research Chair of the Intelligent Integrated Sensors and Antennas, University of Alberta, where he is also a Co-Founder of WiDyne Technologies and SenZioT Technologies. His current mission is to foster a strong collaboration between industry and academia and stimulate more industry relevant research in wireless technologies. The research conducted through this industrial chair program will allow ICT (information and communications technology) innovations to be applied to the areas of intelligent integrated sensors and antennas to improve the productivity of the oil-energy sector and to sustain its growth. He has more than 180 refereed journal and conference articles and several patents in this field. His research interests are in the areas of advanced intelligent antenna, microwave and millimetre-waves circuits and systems, 5G phased array antennas, UWB radar systems, 3-D printing electronics, wearable antennas, and the Zero-power IoT.